Advances in Water Resources 97 (2016) 144–155

Contents lists available at ScienceDirect

Advances in Water Resources

journal homepage: www.elsevier.com/locate/advwatres

Field evidence of swash groundwater circulation in the microtidal rousty beach, France

Damien Sous[a,b,*], Lise Petitjean[a,b], Frédéric Bouchette[c], Vincent Rey[a,b], Samuel Meulé[d], Francois Sabatier[d], Kévin Martins[e]

[a] Université du Sud Toulon-Var, CNRS/INSU, IRD, MIO, UM 110, 83051 Toulon Cedex 9, France
[b] Aix-Marseille Université, CNRS/INSU, IRD, MIO, UM 110, 13288 Marseille cedex, France
[c] GEOSCIENCES-Montpellier, Universit de Montpellier II, Montpellier, France
[d] CEREGE, Aix-Marseille Université, CNRS UMR 6635, Aix en Provence, France
[e] WEIR, University of Bath, Bath, UK

ARTICLE INFO

Article history:
Received 19 April 2016
Revised 16 September 2016
Accepted 16 September 2016
Available online 17 September 2016

Keywords:
Swash zone
Groundwater circulation
Sand beach
Porous media

ABSTRACT

This manuscript reports on a novel field experiment carried out on a microtidal beach in Camargue, France. For the first time in the field, a comprehensive description of the groundwater dynamics under sandy beach swash zone is presented. A cross-shore network of 15 buried pressure sensors is combined with terrestrial LiDAR measurements to study the swash-groundwater dynamics. The presented data focus on the decay of a moderate storm which allows to monitor the evolution of the groundwater pressure field in response to the retreat of the swash zone. Both horizontal and vertical head gradients are measured within the porous sand soil to estimate the groundwater flow field using Darcy's law. Time-averaged analysis demonstrates the presence of a rather consistent groundwater circulation pattern under the swash zone, shifting offshore with the swash zone. The main tendency is an offshore directed flow, with infiltration/exfiltration in the upper/lower parts of the swash zone. Time-resolved analysis highlights the typical groundwater response to swash events which consists mainly of an overall infiltration flow during the bed inundation by the swash tongue, a seaward flow during the swash retreat and, for long backwash events, a localized exfiltration flow under the next incoming uprush.

© 2016 Elsevier Ltd. All rights reserved.

1. Introduction

Since Waddell's early work (Waddell, 1973; 1980), groundwater dynamics in sedimentary beaches has attracted increasing interest during the past few decades due to its implications to a wide range of physical, biological and chemical processes. The beach face being a mobile and porous boundary between land and open sea, the determination of groundwater fluxes is of primary importance to quantify the exchanges of fresh/salt water between ocean, coastal aquifers and lagoons at various spatial scales, from passive margin (Lofi et al., 2013) to the nearshore scale (see e.g. Burnett et al., 2006; Robinson et al., 2006). Groundwater fluxes also control the diffusion of dissolved materials, such as nutrients or pollutants (Anschutz et al., 2009; Sawyer et al., 2014), or the biogeochemical cycles within sedimentary beaches (Charbonnier et al., 2013; McAllister et al., 2015). At smaller scales, through bed percolation flows can affect sediment transport by modifying the swash volume (although only significant for gravel bed), the boundary layer structure (Conley and Inman, 1994; Corvaro et al., 2014a, 2014b) and the relative weight of sediment (Turner and Masselink, 1998). The two latter effects are competing through the sediment grain size: for a fine sand (i.e. grain diameter less than 0.4-0.6 mm), the cumulated effect of in/exfiltration flows on a swash cycle favors offshore transport, while for coarser sand the net transport is onshore (see e.g. Austin and Masselink, 2006; Butt et al., 2001; Chardón-Maldonado et al., 2015; Karambas, 2003).

In the field, the main difficulty in quantifying groundwater fluxes resides in the impossibility, with the current state of technology, to directly measure flow velocities within the porous soil. Subterranean flows within sedimentary beaches or coastal barriers are indirectly carried out at large scale from measurements of watertable fluctuations (Nielsen, 1990; Turner et al., 1997). Finer descriptions of beach groundwater dynamics are alternatively provided by numerical simulations (Li and Barry, 2000) or laboratory experiments (Cartwright et al., 2004; Shoushtari et al., 2015; Sous et al., 2013; Steenhauer et al., 2011; Turner et al., 2016; Turner and Masselink, 2012). Above the intersection between watertable

* Corresponding author.
E-mail address: sous@univ-tln.fr (D. Sous).

http://dx.doi.org/10.1016/j.advwatres.2016.09.009
0309-1708/© 2016 Elsevier Ltd. All rights reserved.

and beach surface, the dynamics of sand saturation in response to waves and tides is quite complex (Turner, 1993). A great insight into infiltration/discharge processes leading to saturation fluctuations at multiple timescales has been brought by recent laboratory (Steenhauer et al., 2011), field (Heiss et al., 2015; 2014) and numerical studies (Geng and Boufadel, 2015). The time-averaged groundwater flow under an active swash zone generally consists in a localized seaward circulation cell which is predominantly controlled by waves action at the beach face. In their large-scale experiment, Turner et al. (2016) additionally observed a flow division near the top of the swash zone: the groundwater flow is seaward under the swash zone and landward beyond the top of the swash zone. They also showed the dominant effect of waves with respect to the weak role played by the variations of back-barrier lagoon water level. The presence of exfiltration flow under or offshore the swash zone has also been observed for both time-averaged or single swash event dynamics (Li and Barry, 2000; Sous et al., 2013; Turner et al., 2016).

Most of the studies of swash-groundwater processes have been dedicated to the characterization of sub-surface pressure gradients (see Horn, 2006 for a review) in the saturated beach or the analysis of saturation dynamics in the upper swash zone (Heiss et al., 2015). The objective of the present paper is to present a first comprehensive field characterization of groundwater dynamics in the permanently saturated area at the whole swash zone scale. In particular, groundwater pressure fields are monitored at high resolution deep in the soil allowing the identification of any deviation to the hydrostatic equilibrium and, consequently, any pressure gradient induced groundwater flow. As a part of a larger nearshore experiment, a swash-dedicated experimental set-up, mainly based on buried pressure sensors and terrestrial LiDAR, has been deployed on Rousty beach in Camargue (France) during the winter season 2014–2015.

2. Field site and experimental setup

2.1. Rousty beach

The studied site is the microtidal Rousty beach located on the Mediterranean coast of France in the National park of Camargue. Hydro- and morphodynamics features of Rousty sand beach have been monitored for 15 years (see Ouahsine et al., 2013; Sabatier, 2001, 2008; Sabatier et al., 2009a, 2009b). Fig. 1 shows a schematic profile of Rousty beach with a typical fair weather swash bar below the berm, while the profile measured during the present experiment, smoothed by the winter wave climate, is displayed in Fig. 2. A nearshore bar, out of scale in Fig. 2, is located at about X = 170 m and Z = -0.8 m in the local datum (see below for details). The mean sediment size is around 200 μm and its distribution is quite homogeneous over the studied area in the 3–4 m surface layer (Sabatier, 2001). Deeper in the soil, harder clay layers have been observed during the tubes burying but a proper characterization would have required coring and seismic analysis, which lies outside the scope of the present paper dedicated to swash processes. No rainfall have been observed during the present campaign and no groundwater or surface fresh water inputs have been identified in the surrounding area (De Montety, 2008). The following analysis of swash zone groundwater dynamics will then be carried out assuming a homogeneous sediment and neglecting any density gradient effects. The tide range is small (around 0.3 m). However, the mean water level shows significant fluctuations, rising to more than 1 m under South-Easterly wind and low atmospheric pressure conditions associated to storms striking the northern Gulf of Lions. Setdown can reach −0.5 m during Northerly (Mistral), North-Westerly (Tramontane) winds and high pressure conditions. Mistral and Tramontane show mean velocities around 11 m/s and maxima greater than 20 m/s. West to South-West winds and South-East winds associated to storms show similar mean and maximal values. Wave climate is bimodal. The most frequent wave conditions (so-called fair weather waves) are short ($T_p < 6$ s), small ($0.5 < H_s < 1$ m) with a dominant incoming direction from South-West. Storm waves are generated by South-East winds and have a typical Mediterranean signature ($H_s > 2$ m and $T_p > 7$ s), i.e. generally short-crested and broad-banded storm waves. The most eastern swells are refracted by the Beauduc spit before entering the Gulf of Beauduc, which reduces (but does not nullify) the wave incidence at the selected site.

2.2. Instrumentation and methods

A sizeable network of instruments has been deployed for three months from November 2014 to February 2015 to characterize the hydro-morphodynamical beach processes during the winter season. The present study focuses on higher resolution measurements of swash zone groundwater dynamics carried out during a ten-day campaign. The analysis proposed here was performed on a nearly continuous 24 h-long acquisition period from December 13, at 9:30AM till December 14, 10:00AM. A moderate storm hit the site during the previous night, allowing a complete inundation of the berm (and thus the measurement area). The period considered in this work corresponds to the storm tail which is, as shown later, of particular interest to monitor the comprehensive groundwater circulation pattern under the swash zone. Before and after this storm, strong offshore winds, high atmospheric pressure and weak wave energy maintained the swash zone away from the instruments.

The set of instruments mainly consisted in 15 buried pressure sensors and LiDAR measurements. The pressure sensors (STS ATM) measure relative pressure in the $0–4\times 10^4$ Pa with a resolution about 10 Pa. The offshore wave forcing is provided by an RDI 600 khz Acoustic Doppler Current Profiler (ADCP, 7 m deep). Two additional (autonomous) pressure sensors were deployed to measure the Mean Water Level (MWL, affected by wave setup) at the end of the inner surf zone and the offshore Still Water Level (SWL, measured at a depth of 7 m, i.e. far from the breaking zone considering the wave conditions). The cross-shore distances from the LiDAR tower are 37.8 and 710 m for the MWL (surf zone) and SWL (offshore) sensors, respectively. Two altimetric surveys were conducted with RTK-DGPS and tacheometer in the morning and in the afternoon of the 13th of December (around 8:30AM and 2:30PM, respectively). An overview of the experimental setup and beach morphology is shown in Fig. 2.

In the following, the vertical coordinate Z refers to the vertical position in the French national reference frame NGF, while the cross-shore horizontal position X is positive seaward and defined, for the sake of simplicity in this swash-focused study, from the LiDAR location (i.e. $X_{LiDAR} = 0$).

2.2.1. Lidar measurements

A 2-dimensional laser scanner (LiDAR) was deployed on a 5m high scaffold structure. Despite of some limitations (Almeida et al., 2015; Blenkinsopp et al., 2010), such instruments are increasingly used to measure, at high frequency and fine spatial resolution, both bed and free surface dynamics over the inner surf and swash zones. In the swash zone, the LiDAR captures a moving interface which is alternatively dry and wet in response to the uprush/backwash cycles. Sand bed elevation can be extracted at each cross-shore position owing to the fact that, when uncovered, the bed sends back a nearly constant signal. The LiDAR angular resolution is 0.1667^o leading to a spatial resolution between 1 and 2 cm in the considered area. All details of the present setup and data processing can be found in Martins et al. (2015).

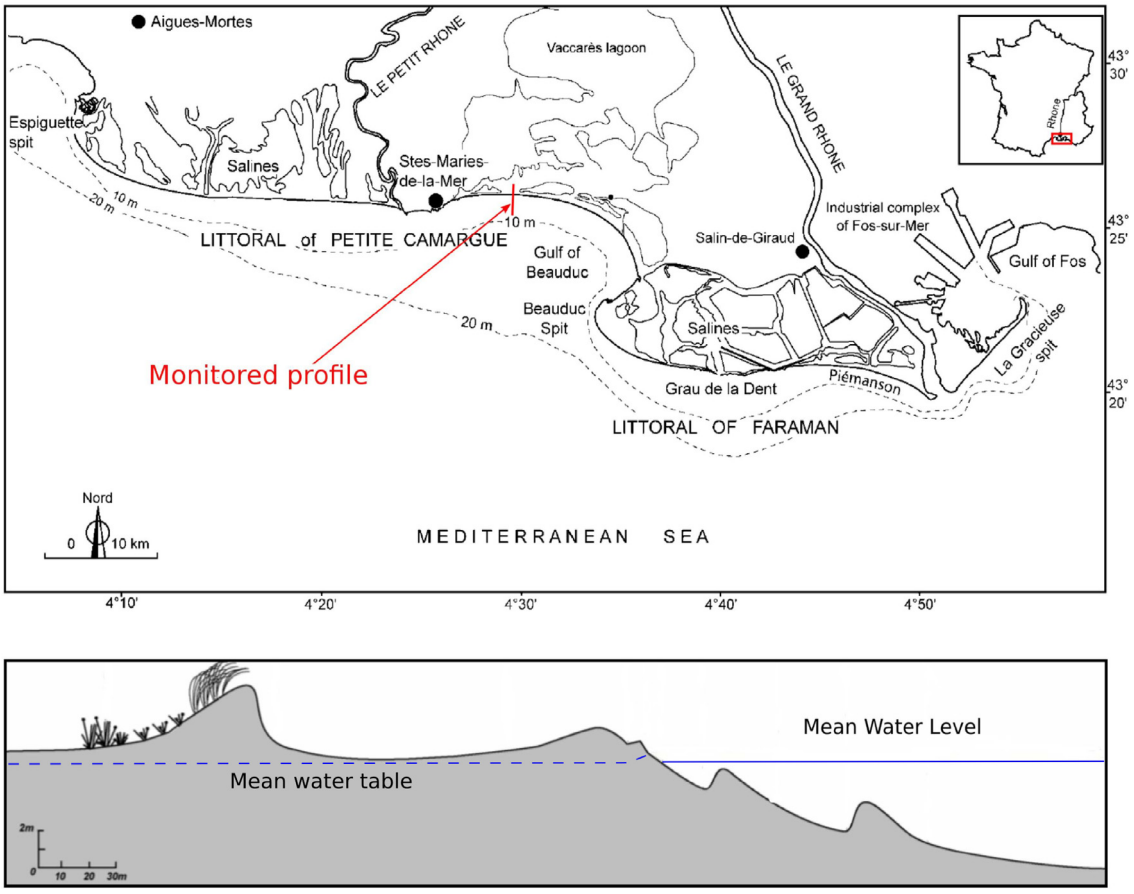

Fig. 1. Site location and typical beach profile (from Sabatier, 2001). Indicative mean water and groundwater table elevations are depicted for typical fair weather conditions, with the expected humped watertable shape under the swash zone.

For illustration purpose, Fig. 3 shows the bed time evolution for five selected cross-shore positions (the positions of each pressure sensor, see Fig. 2). Offshore (SWL) and surf zone (MWL) mean water levels as well as offshore wave forcing (over successive 30 min bursts) are also depicted. An erosive trend occurs during the first three hours of measurements; then tendency changes to accretion at each position. More precisely, it is observed that bed in the swash zone is strongly affected by the mean water level (MWL) fluctuations. As long as the considered position is affected by swash motions, each MWL increase is related to a decrease of the bed elevation. In addition, the comparison of MWL and SWL (Still Water Level measured at the offshore pressure sensor) evolutions displayed in Fig. 3 shows the combined influence of waves and tides in the free surface dynamics; the wave setup varies from 13 to 5 cm as the significant wave height decreases from 1.8 to 0.8 m.

2.2.2. Pressure measurements

The study of the groundwater swash zone is performed by means of a network of 5 vertical poles equipped with 15 pressure sensors named G1t to G5b (3 pressure transducers per station, see Fig. 2): the number indicates the cross-shore position of the pole while the letter denotes the vertical position (t, m and b for top, middle and bottom, respectively). Spirit-level measurements in both cross-shore and longshore vertical planes have been performed along each pole during burying to ensure the vertical alignment of the pressure sensors. Uncertainties of this method are estimated to be lower than 1%, which is of the same order of accuracy than the pressure sensors measurements. The sensors were protected by a sediment net to prevent sediment infiltration and sensors membrane damage (Turner and Nielsen, 1997). The sensors were set with upward facing membranes in order to easily vent the protective shelter. They measure relative pressure thanks to a capillary tube which brings atmospheric pressure into the sensor. As long as the sand medium around the sensor is saturated, these pressure sensors can virtually measure negative relative pressure, i.e. absolute pressure lower than atmospheric pressure. All sensors were time-synchronized through a robust time triggering system on a laptop located onto the scaffold structure, where data were logging at the sampling rate of 10 Hz. Each sensor was positioned by DGPS and repeatedly calibrated in laboratory basin both before and after the experimental campaign. The calibration is performed in hydrostatic conditions by immersing the pressure sensors in water bassin at rest, at variable depths (from 0.1 to 1.2 m, each 0.1 m). The drifts of the sensors offset were controlled using atmospheric pressure measurements before and after the experiment and, if needed, compensated. Similar procedure is used for the autonomous pressure sensors (OSSI Wave Gauge, range 0–10 m, resolution about 5 mm) dedicated to MWL and SWL measurements. Piezometric head and both vertical and horizontal pressure gradients are calculated inside the sand soil. The relative pressure measurements are in the range $0 - 4 \times 10^4$ Pa with a resolution of about 10 Pa. For each sensor, the pressure head h (simply called head hereinbefore) is calculated as $h = P/\rho g + Z_c$ where P is the measured relative pressure, ρ the water density and Z_c the sensor elevation.

Any departure from the hydrostaticity within the soil is expected to induce groundwater flows, provided that the water flows in the direction of decreasing fluid potential as stated by Darcy's

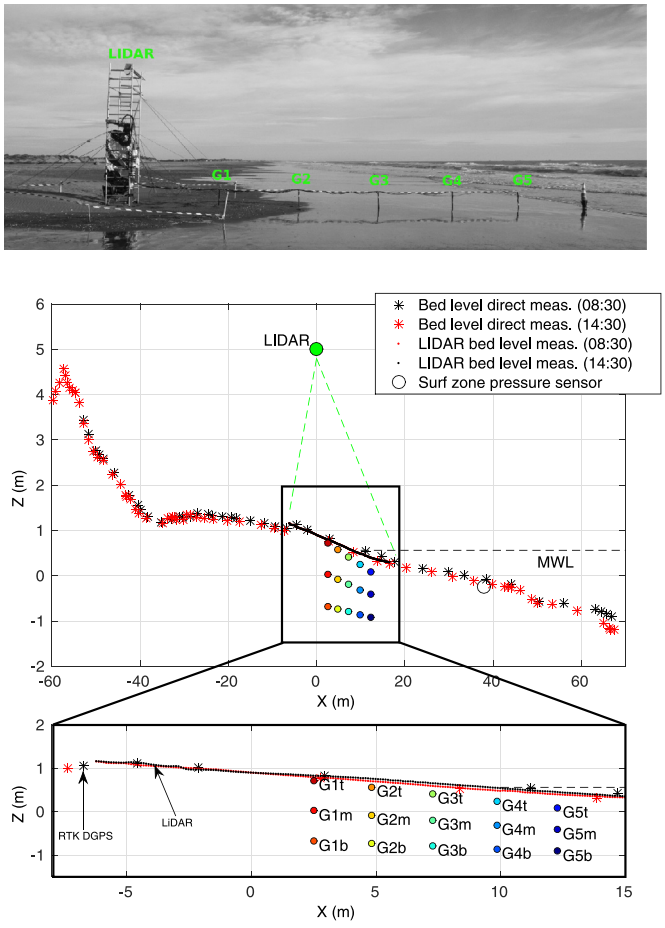

Fig. 2. Description of beach cross-shore profile and experimental setup. Top plot is an overview picture taken after the storm. In middle and bottom plots, red and black stars represent the bed level direct measurement by DGPS while red and black dots depict the LiDAR measurements (which appear nearly continuous at the present scale). The large black circle indicates the position of the MWL surf zone pressure sensor. The SWL sensor is far offshore (X = 710 m). (For interpretation of the references to colour in this figure legend, the reader is referred to the web version of this article.)

law. Velocity is thus estimated from the head field as follow:

$$\vec{V} = -\frac{K}{\rho g}\vec{\nabla}P \tag{1}$$

where $\vec{V}$ is the 2D (vertical plane) velocity field, ρ the water density and g the gravity acceleration. The hydraulic conductivity K is estimated at 0.016 cm.s^{-1} using a series of falling head tests (Klute and Dirksen, 1986) from 3 differents samples taken at the sand surface along the studied area.

In order to analyse the overall groundwater pressure and velocity fields from discrete measurements points, a triangulation-based natural neighbour interpolation is applied on the pressure data (Sibson, 1981). The choice of a proper interpolation method is not straightforward, in particular in the present case where the vertical spacing between sensors is smaller than the horizontal one. A series of tests has been carried out to compare the interpolated fields provided by four interpolation methods: linear, natural neighbour and cubic triangulations-based and bi-harmonic spline interpolations (MATLAB® 4 method). In addition to a qualitative analysis of the consistency of the resulting fields, a quantitative criterion based on the field divergence is used. Our physical system being long-shore uniform both in terms of hydrodynamical forcing and sediment features, the groundwater circulation is assumed to be also long-shore uniform, at least at the considered scales. This implies that the divergence of groundwater pressure field (in the vertical plane) should be minimal. For the considered data, the natural neighbour interpolation method has systematically produced the more regular results, evaluated in terms of mean and maximal values as well as the standard deviation of the divergence field, and is thus retained for the calculation of the pressure field over a regular grid.

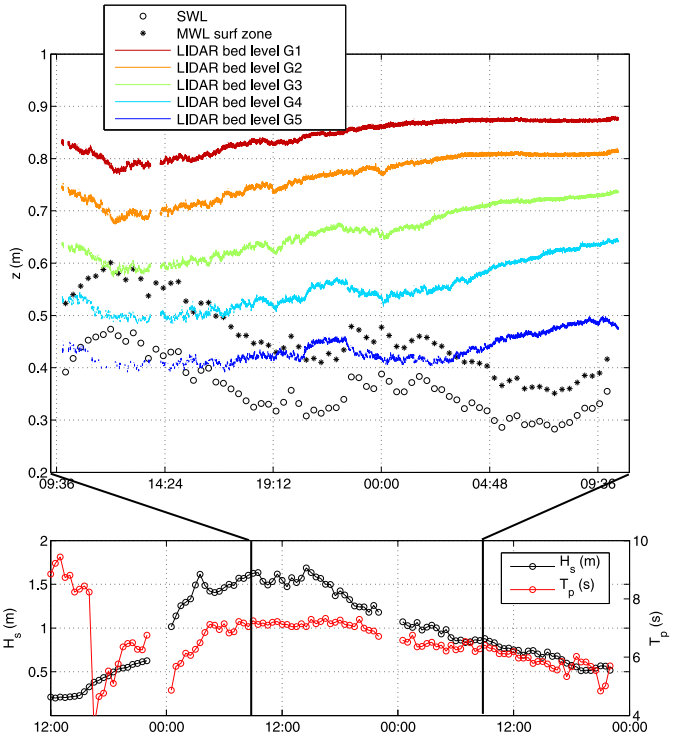

Fig. 3. Top: LIDAR bed level measurements above G1, G2, G3, G4 and G5 sensors and time-averaged water level for offshore (SWL) and surf zone (MWL) pressure sensors. Bottom: offshore wave features over the whole storm event.

3. Results

3.1. Measurements overview

A first overall insight on the data is provided by Fig. 4. The top panel (A) shows the temporal evolution of the MWL in the surf zone and of the 20 min averaged head at each sensor. It is first observed that, excepted at the most offshore station at the swash base, the watertable is higher than the surf zone MWL. This is consistent with observations of runup elevating the mean water table under the swash zone (Kang et al., 1994; Turner et al., 1997). The heads measured at the inland sensors are generally higher than those measured seaward. This observation is consistent with the fact that, as long as the watertable remains attached to the sand bed, it follows the seaward lowering of the mean beach topography in the swash zone. Such trend is not clear when the watertable falls below the sand bed, as observed during the last part of the measurement period for the G1-G2 stations (see Fig. 4, A, after 3AM) for which a zero-gradient situation (nearly flat watertable and hydrostatic equilibrium) is measured as discussed later on. The first-order time decrease of each head over approximately 24 h clearly originates from the reduction of the wave forcing (H_s from 1.8 m to 0.8 m; T_p from 7.5 s to 5.6 s) and the decrease of regional setup (SWL lowering about 15 cm) during this period. In addition, each head falling clearly follows, with a variable magnitude, two successive patterns of approximately 12 h each. This second-order head oscillation obviously results from the coupling

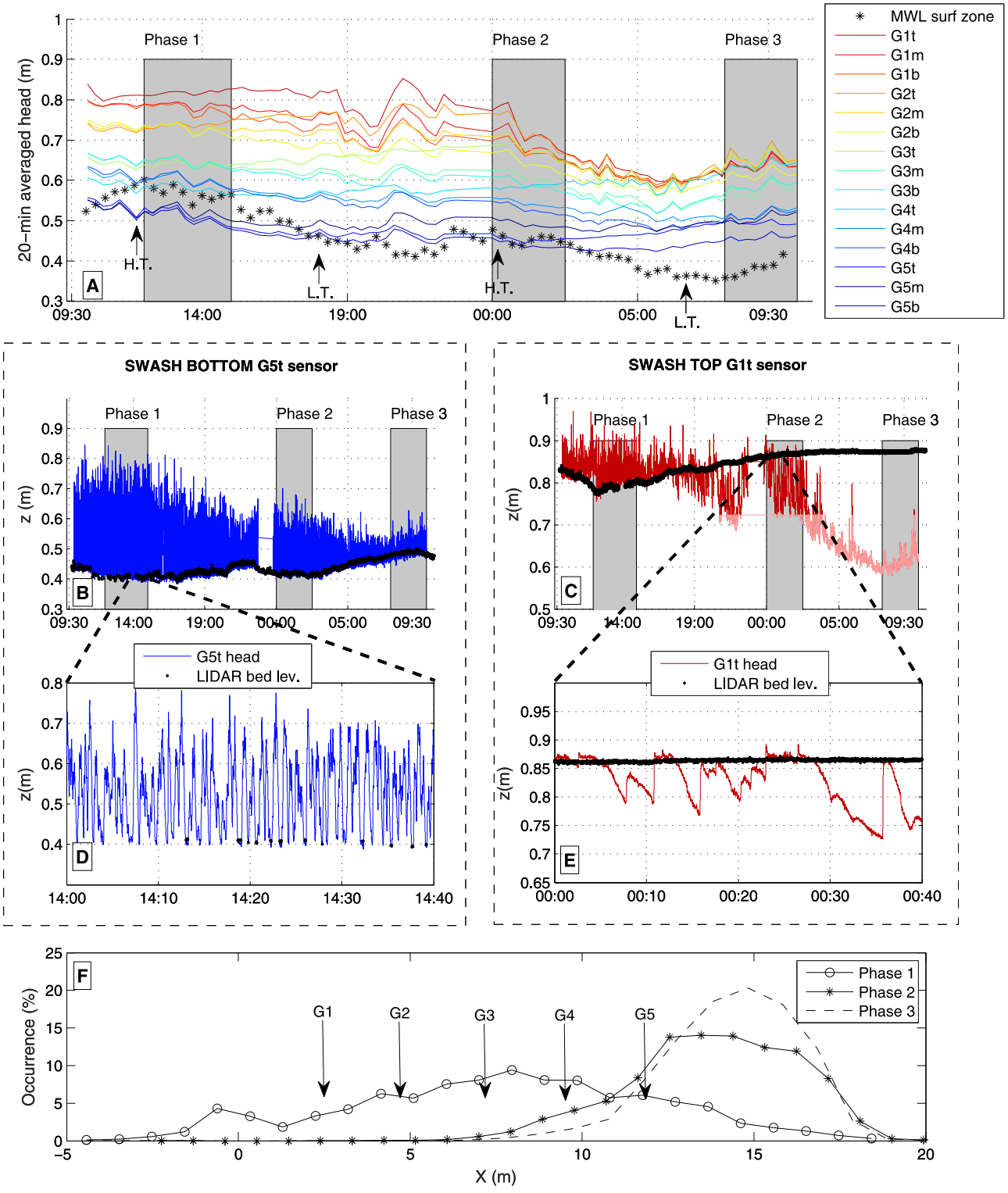

Fig. 4. A: 20 min averaged head at each sensor (colored lines) and surf zone MWL (black flakes), with black arrows indicating high (H.T.) and low (L.T.) tide. B and C: G5t and G1t instantaneous head and LiDAR bed level over the entire dataset (light red line corresponds to measurements performed above the watertable, see text). D and E: G5t and G1t instantaneous head and LiDAR bed level for selected 40-min periods. Note the sparser LiDAR measurements due to rarer drying backwash events. F: probability density for the cross-shore position of the swash front for the three selected periods (vertical arrows indicate the cross-shore position of pressure sensors). (For interpretation of the references to colour in this figure legend, the reader is referred to the web version of this article.)

of the tide excursion (M2 semi-diurnal harmonic component of the order of 20 cm) with the first order tendency. While difficult to interpret in all details oscillations of higher frequencies, head dynamics during the experiment display subtle differential evolutions of neighbouring sensors which drive both horizontal and vertical pressure gradients within the sand soil. In order to highlight the evolution of the groundwater pressure field in response to the global offshore shifting of the swash zone, we select three characteristic 3-hour long periods referred to as Phases (grey block in Fig. 4). Phases 1 and 3 are representative of typical groundwater

states associated to high and low swash zones, respectively. They are largely depicted herein after. Phase 2 illustrates a transitional state between phase 1 and phase 3.

Head timeseries for G1t (swash top sensor) and G5t (swash bottom sensor) sensors are presented in Fig. 4. Panels B and C show the entire measurement dataset while panels D and E focus on selected 40 s period for G1t and G5t sensors, respectively. These zoomed plots, which are detailed below, help to build up a better idea of the collected groundwater pressure data. In addition, bed level measurements by LiDAR are plotted in black dots. To better identify the swash zone extension during the three phases, the occurence probability of the cross-shore position of the swash front has been extracted from LiDAR data and plotted in Fig. 4 F. The cross-shore locations of pressure sensors are indicated by arrows. During phase 1, the MWL is high (above 0.5 m), the watertable coincides with the sand bed for each sensor and the uprush events largely extend beyond the studied area and cover each sensor. Phase 2 shows the retreat of the swash zone with only 5% and 1% of inundation periods reaching G4 and G3 positions. This trend is even more pronounced for phase 3 with 1.7% and 0.3% of swash events inundating at G4 and G3 sensors.

The G5t head highlights the watertable dynamics in response to the decrease of the MWL in the lower part of the measurement area (see Fig. 4 B–D). All along the experiment, the G5t sensor is driven by regular infragravity swash events. Backwash events are rarely long enough to allow the dry sand bed detection by LiDAR (showed as black dots in Fig. 4B). One can however note that, for the available bed level data, the agreement between bed position measured by LiDAR and G5t head measurement is very good, the discrepancies being explained by the slightly different monitored cross-shore profile and the unknown head gradient between the pressure sensor and the sand bed. This indicates that sand remains always saturated and the watertable attached to the sand bed.

In the upper part of the measurement area, the G1t sensor shows a radically different behaviour (Fig. 4 C–E). Following the swash zone retreat, the sand bed becomes here increasingly exposed during backwash events, allowing more regular LiDAR bed level measurements. From 9:30AM to 5:30PM, the pressure dynamics is similar to the one observed for the G5t sensor (see above). The subsequent decrease of MWL and wave activity induces a retreat of the swash zone. This is illustrated in Fig. 4F: during Phase 2 only very rare and thin uprush events are able to inundate the G1 position and for Phase 3 the swash zone has receded even much lower. This evolution is associated to a progressive lowering of the watertable which falls behind the bed level during the longest backwash events, as demonstrated in Fig. 4E. The asymmetric low frequency oscillations (rapid rise and slow fall) denote typical capillary fringe fluctuations. Note that during the last part of the experiment, the watertable falls up to 10 cm below the G1t sensor which corresponds to negative relative pressure. However, such measurements, which are depicted in light red in Fig. 4C, should be analysed with caution as the groundwater pressure field above watertable is still poorly documented for the sandy beach swash zones. For a more detailed insight of the physical processes driving groundwater pressure fluctuations under the swash zone, the reader is referred to the sounding analysis of Turner and Nielsen (1997) and earlier groundwater works (Hegge and Masselink, 1991). Nevertheless, one notes here that the pressure field at the G1 pole remains remarkably hydrostatic (see Fig. 4, A, Phase 3 or Fig. 5, bottom plot) even few centimeters above the watertable.

3.2. Time-averaged dynamics

Fig. 5 depicts the time-averaged head and velocity fields computed over the three selected phases (see Fig. 4). Data are time-averaged over 3 h acquisition periods. Maximal velocity magnitudes are 1.5 10^{-5}, 1.4 10^{-5}. and 2.4 10^{-5} m/s for the top, middle and bottom plots, respectively. Sand bed elevation measured by LiDAR and tacheometer on December 13, are shown as well as the locations of buried pressure sensors. The cross-shore position of the swash zone for the selected time period can be found in Fig. 4, F.

The measurements presented in Fig. 5 indicate the presence of a rather consistent groundwater circulation pattern under the swash zone, which shifts offshore as the swash zone retreats with the lowering of MWL. Phase 1 (Fig. 5, top plot) is characterized by a very high swash zone. The measurement area is here under the lower part of the swash zone. The main tendency is a offshore directed groundwater flow. In more details, one notes the presence of a groundwater circulation cell, with a strong infiltration at the inland sensor and an upward directed exfiltration flow under the base of the swash zone. During Phase 2, both MWL and watertable decrease and the swash oscillations occur in the zone $7 < X < 19$ m (see Fig. 4, F). Strong infiltration is still observed but it now extends to most of the measurement area. An offshore-directed velocity component is also present, but weaker than during Phase 1. Phase 3 (Fig. 5, bottom plot) is characterized by an even more compact swash zone and a much lower watertable. The groundwater pressure becomes nearly hydrostatic in the inland region which is no more affected by uprush events. The flow under the swash zone is nearly a downward infiltration flux.

As predicted by previous analytical (Longuet-Higgins, 1983), numerical (Li and Barry, 2000) or laboratory works (Turner et al., 2016), the time-averaged beach groundwater flow in the presence of waves is mainly driven by wave setup and swash uprush. A hydraulic gradient develops across the beachface, resulting in infiltration at the upper swash and exfiltration at the lower swash. The vertical extension of this circulation cell is likely dependent on the presence and the depth of an impervious layer deeper in the soil which cannot be captured by the present instrumentation.

3.3. Statistical properties

The analysis of statistical properties of groundwater dynamics is performed during Phase 1 since most of the instrumentation is affected by the swash motion during this phase. Fig. 6 shows the head energy spectrum for top and bottom groundwater pressure sensors, surf zone and offshore wave measurements, computed over the first 30 min of Phase 1. The evolution of the energy distribution in the frequency domain from the forcing, i.e. the incoming swell, to the different measurement groundwater stations is important to understand how and where free surface oscillations are forcing the groundwater flow within the porous media under the swash zone. One notes first the successive transformations of the energy spectrum from offshore measurement (red thick line) where energy is concentrated in the incoming swell band (T_p at 8.3 s), at surf zone sensor (black thick line) where most of the energy has been transferred in the infragravity band (with two peaks around $T_p = 35$ and 140 s) and, finally, at the buried pressure sensors for which groundwater head fluctuation energy is nearly negligible above frequency 0.06 Hz. A remarkable feature in the distribution of infragravity energy is the difference between the swash and surf zone measurements. The trough observed for the surf zone sensor around 0.017 Hz can be explained by the presence of a standing wave trapped between the shoreline and the shallow inner bar (bar top around -0.6 m at 70 m seaward the shoreline). The seiche theory with the simple hypothesis of a 1D flat sloping bottom basin of 70 m length (Wilson, 1972) predicts a fundamental mode of basin oscillation at 0.0156 Hz, which nicely fits with the observation. Around this frequency, the swash pressure sensors ($2 < X < 12$ m) are thus exposed to a seiche anti-node

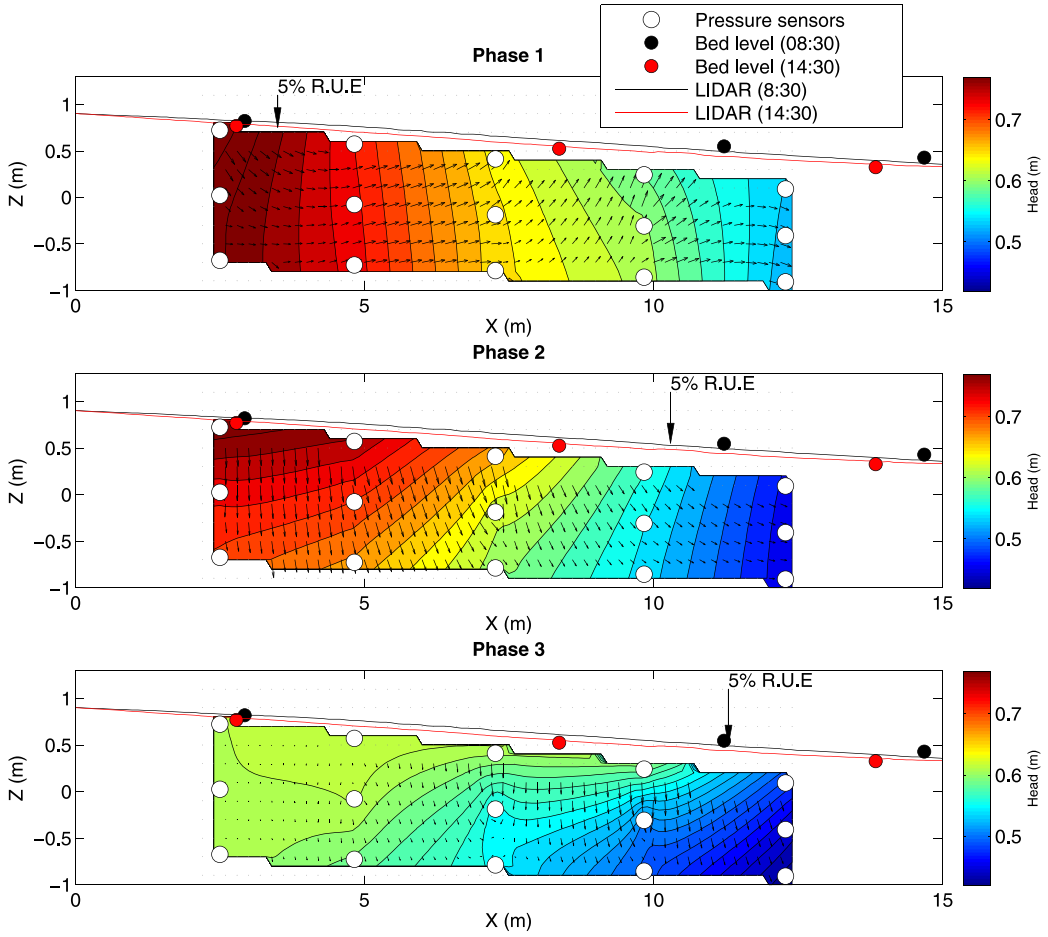

Fig. 5. 3 h time-averaged groundwater head contours (in m) and estimated velocity field for the three selected periods (top: Phase 1, middle: Phase 2, bottom: Phase 3). Maximal velocity magnitudes are 1.5 10^{-5}, 1.4 10^{-5}. and 2.4 10^{-5} m/s for the top, middle and bottom plots, respectively. Vertical arrows indicate, for each phase, the 5% Run Up Exceedence i.e. the most inland cross-shore location reached by 5% of the uprush events on the selected period.

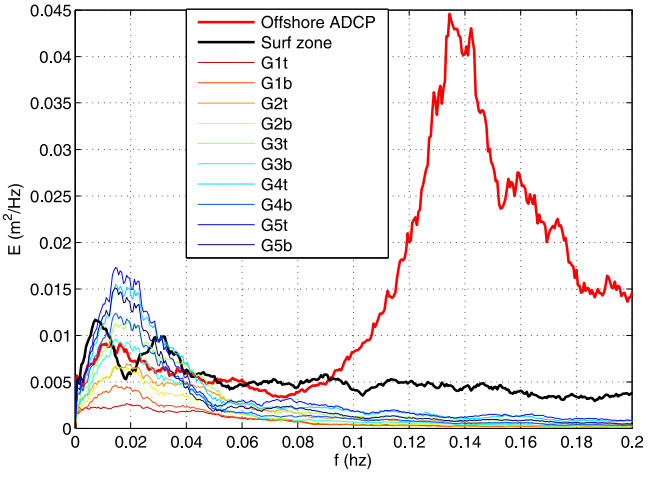

Fig. 6. Energy spectrum for top and bottom groundwater pressure sensors, surf zone and offshore wave measurements.

(i.e. maximal amplitude) while the surf zone pressure sensor (X = 37.8 m), located nearly half way to the bar (bar top around X = 90 m), measures minimal amplitude associated to the standing wave node. A more careful characterization of long wave dynamics has to be carried out to confirm these resonance processes on our bathymetric profile, but it is out of the scope of the present paper and will be the subject of a future work.

The main trend observed in Fig. 6 is that in the groundwater pressure field fluctuates in the same frequency range than the free surface in the overlying infragravity-driven swash zone. The spectra of head fluctuations show the expected cross-shore evolution: the more landward the measurement in the swash zone, the smaller the remaining energy. One notes also the low-pass filtering role played by the sand soil for G3, G4 and G5 sensors, the bottom sensors showing generally weaker energy than the top ones. This trend tends to reverse higher on the swash in particular for the G1 sensors. At this position, measurements shows that the groundwater pressure fall during long bed-drying backwash events is greater deep in the soil than just beneath the sand surface, producing higher head fluctuations. The G1t sensor shows a peculiar spectrum in Fig. 6, with an absence of energy peak around 0.02 Hz and an increasing energy toward lower frequencies.

The spectral analysis of groundwater head fluctuations helps to understand how free surface wave energy propagates into the soil but does not give a direct insight on the groundwater flows since these latter result also from phase shift of pressure waves. To get a better understanding of the pressure-induced flows within the soil, occurrence probability for each sensor pair (both horizontal and vertical) are computed for the three selected Phases and are depicted in Figs. 7 and 8.

It is recalled here that during Phase 1 the swash zone is quite high, which allows to monitor a large portion of the groundwa-

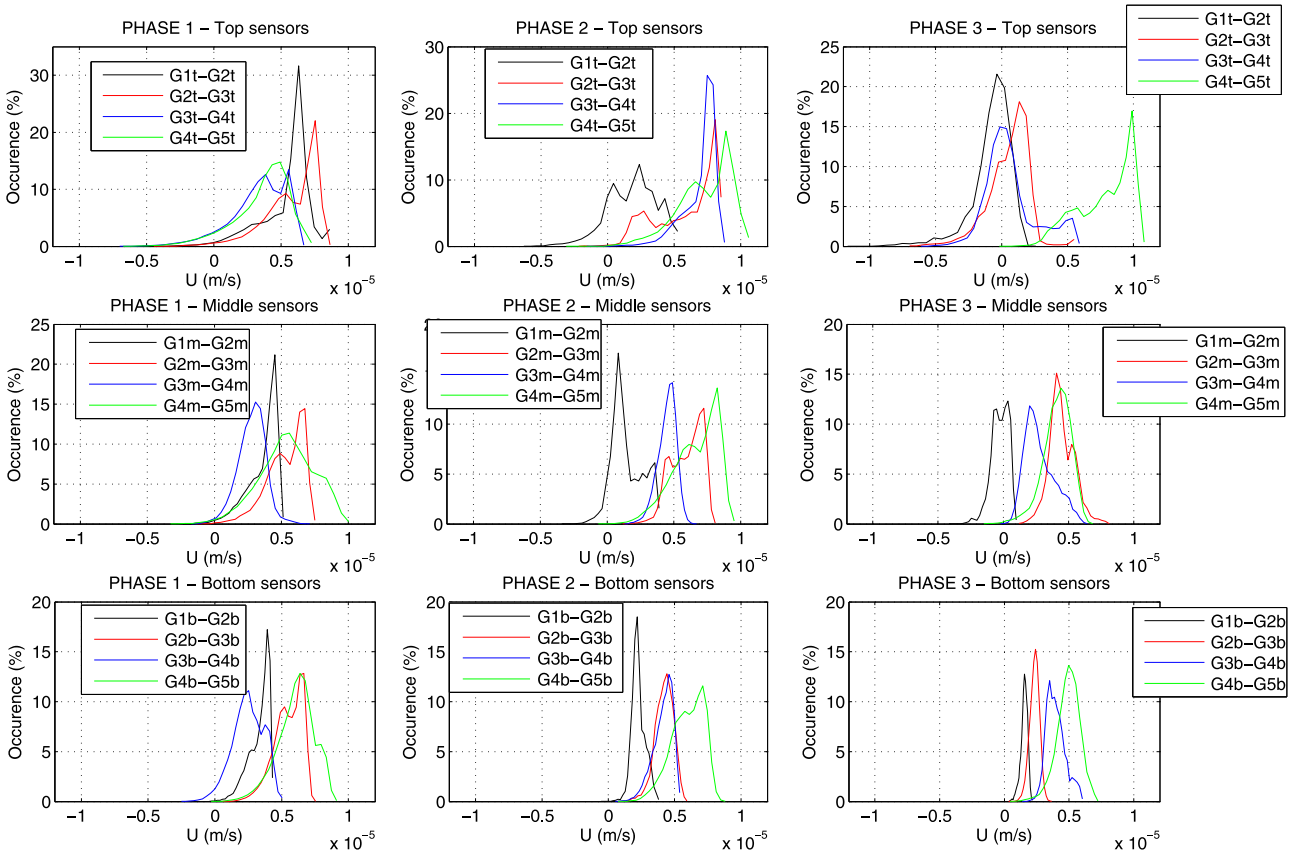

Fig. 7. Probability density for horizontal velocity component for each sensor pair.

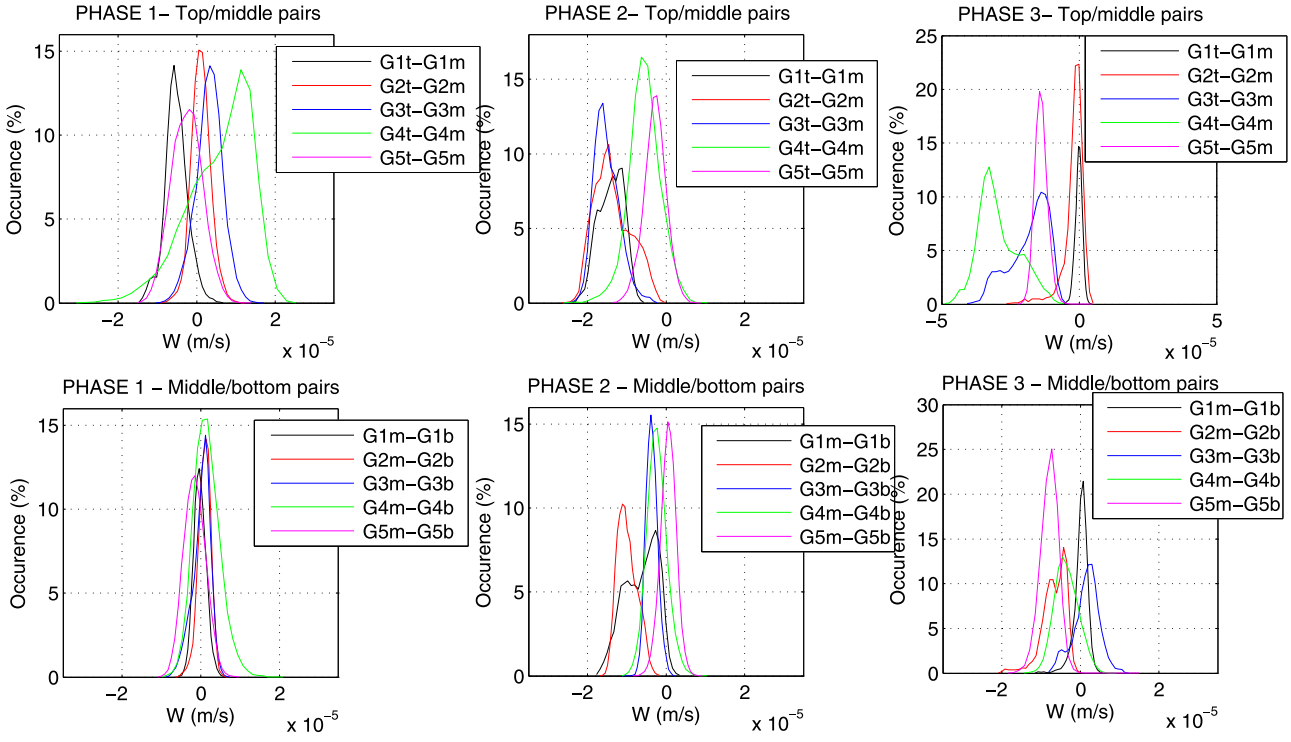

Fig. 8. Probability density for vertical velocity component for each sensor pair.

ter circulation by the deployed setup. When the swash zone progressively lowers during Phases 2 and 3, the circulation cell, which shifts seaward, is truncated and the sensors network mainly captures the infiltration area at the swash top and the nearly hydrostatic region further landward. Rather than commenting separately on each plot, an overall analysis is carried out in order to list the main trends and to map the groundwater velocity field under the swash zone.

- Vertical flows are generally greater than horizontal ones.
- The horizontal velocities are overwhelmingly positive (seaward). The maximal values are generally reached under the middle and upper swash zones and near the sand surface. Under the lower swash, the horizontal component is smaller but the situation is opposite with higher velocities deeper in the soil.
- The vertical flow are generally negative (infiltration) under the upper swash zone and positive (upward) under the lower swash zone. The greater values are observed near the sand bed.
- Beyond the uprush limit, both horizontal and vertical velocity distributions are nearly symmetric. In this case, the measurements are performed landward of the typical swash groundwater circulation pattern and the observed velocities are then related to the propagation of pressure waves in a nearly hydrostatic groundwater field rather than driven by uprush infiltration and wave setup processes. The only exception to this general scheme is found deep in the soil, where small constant seaward directed flows are still observed.

3.4. Time-resolved swash events

During the experiment, the swash zone hydrodynamics was mainly driven by infragravity waves. As such, swash events generally appear as combination of incoming bores. For the sake of clarity, two well-defined swash events are selected during Phases 1 and 3 to highlight the difference in the groundwater response. The first has been observed on December 14, from 14:11:03 (see Fig. 9) while the second is recorded on December 14, from 9:11:35 (see Fig. 10). The period of these events is about twice that of the offshore wave peak period but smaller that the shortest infragravity mode.

It is first observed that, in agreement with the time-averaged circulation depicted in Fig. 5 (top and bottom plots), the initial groundwater conditions between the swash incoming are quite different. For the first event (measured during Phase 1), the watertable is attached to the sand bed, the overall pattern is infiltration in the upper part of the studied area and exfiltration under the base of the swash zone. As the swash tongue covers the swash zone (see snapshots at 14:11:06 and 14:11:10), positive head gradients spread all over the area and induces an overall downward flow trend. At the end of the swash cycle, backwash (14:11:20) is associated to a generalized seaward flow. Note that a slight overpressure is observed for G4m sensor, which is probably a small measurement artifact.

The second swash event (measured during Phase 3) depicts quite different dynamics. The initial conditions at the swash arrival are characterized by a lower watertable, a nearly hydrostatic state under the upper area and a positive head gradient (downward flow) under the lower area. In relation to the MWL lowering observed in Fig. 4, the swash uprush only reaches the center of the measurement area ($X = 7.3$ m). As already described for the first, this swash event induces a main infiltration tendency in the sand soil but it is here clearly limited to the submerged part of the beach face, the inland sensors remaining nearly in a hydrostatic equilibrium. It is also interesting to note the time delay between swash passage and flux within the sand: the maximal infiltration velocity seems to occur after the swash tongue retreat. It is recalled that in that case, the watertable is much lower than the sand bed for each sensor excepted the most seaward pole. The head increase observed for the upper sensor should then be attributed to a rapid rise of the watertable in response to the pressure wave (Turner and Nielsen, 1997).

4. Discussion

For the first time from an in-situ dataset, the present study demonstrates the presence of a time-averaged seaward directed circulation cell under the swash zone, which is mainly driven by both wave activity and water level fluctuations (wave setup) at the beachface. These results are consistent with existing prototype-scale laboratory (Turner et al., 2016) and numerical (Li and Barry, 2000) datasets. In addition to good qualitative agreement with these studies, the groundwater velocities calculated from in-situ buried pressure sensors range in the same (non-dimensional) orders of magnitude.

A key issue is how and to what extent this swash groundwater circulation would be affected by back-barrier lagoon water level fluctuations which induce, in nature, watertable gradients of smaller amplitude than those imposed by swash runups on the beach face (Turner, 1998). The common intuition is that, when the MWL is high compared to the inland watertable (rising tide or storm surge), landward groundwater flow are promoted while the reverse is expected when the MWL is low (falling tide or storm decay). This has been clearly demonstrated in the laboratory in the absence of waves (Turner et al., 2016). However, the remaining question is to assess in which conditions these hydraulic gradients would be strong enough to modify the swash driven circulation pattern in the presence of wave at the beachface. Numerical simulations of Li and Barry (2000) and laboratory experiments of Turner et al. (2016) precisely studied the effect of the landward groundwater conditions on the swash driven groundwater flow. They both show the persistence of the general groundwater flow pattern, i.e. a circulation cell with infiltration at the upper swash and exfiltration at the lower swash, regardless the artificially imposed seaward- or landward-directed hydraulic gradients across the barrier. However, an important disagreement exists between those studies on the possible controlling influence of the landward groundwater conditions on the swash-driven flow: Turner et al. (2016) observed a swash groundwater circulation nearly isolated, from a hydrodynamic point of view, from back-barrier fluctuations while Li and Barry (2000) stated, from their numerical simulations, that the landward height of the watertable controls the cross-shore location of the divergence point in the groundwater velocity field at the top of the swash zone. While the present dataset does not allow to conclude in one way or the other, it is interesting to note that, if both laboratory experiments and numerical simulations predict the presence of a flow division near the uprush limit, it has not been observed in our field experiment. The present in-situ measurements rather reveals the presence of a nearly hydrostatic groundwater region beyond the uprush limit. This should likely be attributed to, (i), the effect of a high inland watertable in this storm decay context inhibiting the formation of landward gradients beyond the swash top and, (ii), to the spatial limitation of the present dataset. Furthermore, this can explain the difference observed between our field data and the experiments of Turner et al. (2016) or the simulations of Li and Barry (2000) about the shape of the groundwater circulation. Indeed, taking a closer look at the time-averaged groundwater velocity field measured here, one notes that the inflow and outflow occur (Fig. 5, Phase 1) are more symmetric than the laboratory or numerical ones, which can again be explained by the role played

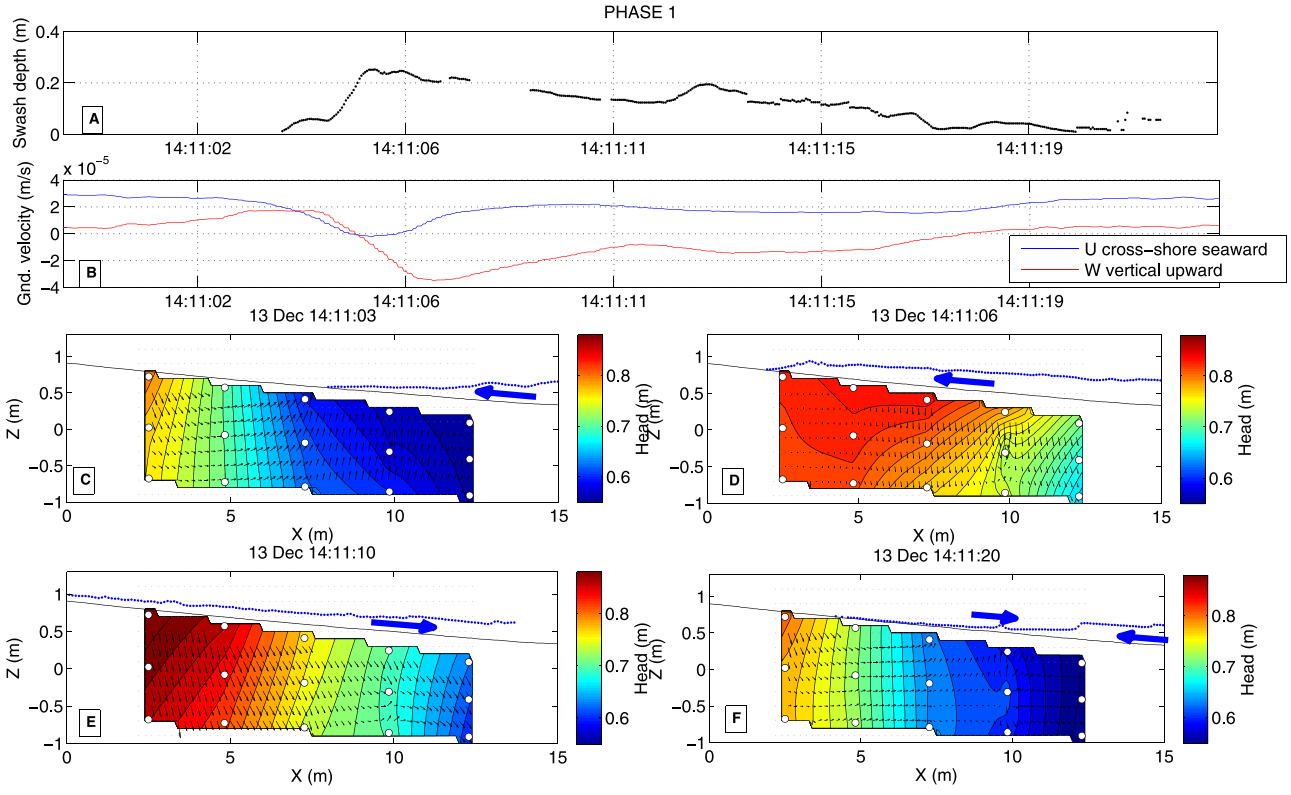

Fig. 9. A: Swash depth measured by LiDAR at $X = 7$ m. B: velocity components extracted at $X = 7$ m, $Z = 0.1$ m. C-F: Snapshots of groundwater head contours and estimated velocity field for a swash event measured during Phase 1. Thick dashed line indicates the estimated watertable position using head data of the top sensors except for G1 pole where G1m is used.

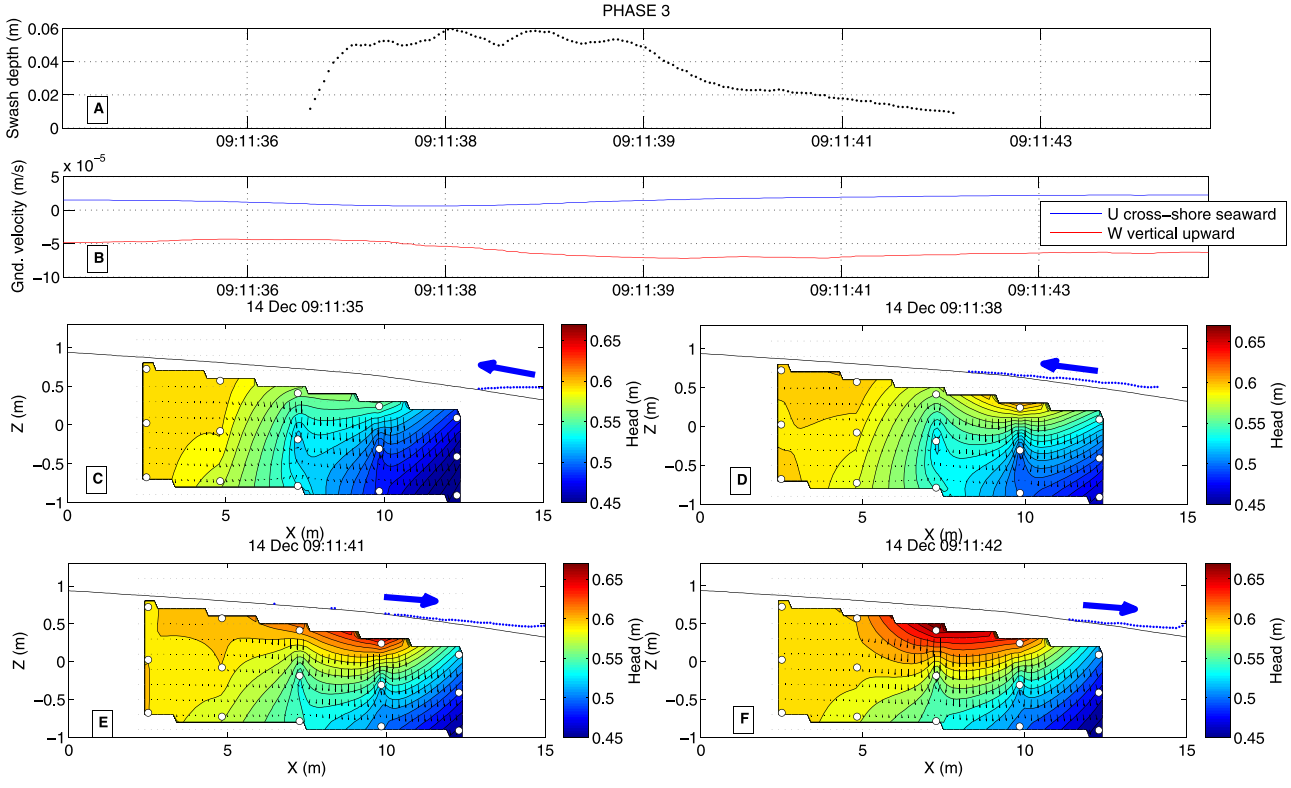

Fig. 10. A: Swash depth measured by LiDAR at $X = 11$ m. B: velocity components extracted at $X = 1$ m, $Z = -0.1$ m. C-F: Snapshots of groundwater head contours and estimated velocity field for a swash event measured during Phase 3. Thick dashed line indicates the estimated watertable position using head data of the top sensors except for G1 pole where G1m is used.

by the inland watertable as suggested by Li and Barry (2000). Additional long-term cross-barrier groundwater data have been recovered further landward and will be processed to test these hypotheses.

At the individual swash event scale, previous field and laboratory measurements as well as numerical simulations have already demonstrated the presence of cyclic infiltration/exfiltration cycles (Butt et al., 2001; Karambas, 2003; Turner and Masselink, 1998; Turner and Nielsen, 1997), but the focus has been systematically made on near bed pressure dynamics in order to quantity an expected impact on the sediment transport. Simple models confronted with the field data generally fairly reproduce the infiltration under the main swash zone and the exfiltration during backwash (Karambas, 2003; Turner and Masselink, 1998) but did not show the infiltration observed just before the bore arrival in the present experiments. More advanced models, such as the one presented by Li and Barry (2000), have been able to capture precisely the groundwater dynamics below the bore front and, more generally, compares very nicely with the present field results.

In the present research work, the experimental setup has been designed to study the groundwater dynamics within the saturated region of the beachface. Moreover, the experimental conditions encountered during the storm decay, which are fairly similar to a falling tide with a high watertable compared to the mean water level, does not provide valuable data on unsaturated processes. During Phase 3, the watertable has been observed to fall about 12 cm below the G1t sensor but the behaviour remains that of a hydrostatic equilibrium scarcely disturbed by groundwater pressure waves and associated capillary fringe effects. In particular, no dual pathway system has been measured, as those observed by in the laboratory (Steenhauer et al., 2011) and in the field (Austin and Masselink, 2006; Heiss et al., 2015).

In addition to the groundwater flow pattern itself, the knowledge of groundwater discharge is of great importance to better understand the exchange and mixing processes within the beach. Considering the averaged groundwater circulation observed in Fig. 4, A, one can estimate the daily seaward groundwater flux around 5 m^2 per longshore beach meter. For a several kilometres long beach, such as Rousty, this can lead to considerable water volumes flowing under the swash zone. However, as the observed circulation cell is rather compact, the impact in terms of exchanges between the beach aquifer and the open ocean may be much smaller. This again recalls the need to understand, at a larger scale, the role of cross-barrier gradients on the swash-zone groundwater exchanges. Obviously, such estimates of groundwater fluxes rely on the assumption of a substantial longshore uniformity of all dynamics at hand. Although the studied site at Rousty beach has been selected to be as longshore uniform as possible, longshore effects are not documented by our experiment and the present discussion must be viewed in this limited context.

At the swash event scale, the present data allows to carry out a simple but original comparison between the discharges observed above and under the sand bed. A specific swash event with a moderate amplitude has been selected during phase 1 in order to monitor the complete event with the present setup. The swash discharge (per beach meter) is calculated dividing the swash volume at the maximal uprush location by the time between the swash arrival in the measurement zone and the time for maximal uprush. It is about 0.75 m^2/s for the considered event. The groundwater horizontal and vertical discharges are averaged over the whole swash event through horizontal ($Z = 0.1$ m) and vertical ($X = 7.5$ m) cross-sections, respectively. This leads to negative downward vertical discharge about 7.10^{-6} m^2/s while horizontal discharge are seaward and about $2.5.10^{-6}$ m^2/s. The surface flux is thus five orders of magnitude greater than its groundwater counterpart. Such ratio should obviously strongly depend on the sand medium properties and rapidly decreases with increasing sediment diameter.

5. Conclusion and prospects

This paper aims to present original field data of groundwater dynamics underneath the swash zone. The 24h swash zone dataset was recorded during a larger field experiment on the microtidal Rousty sandy beach, Camargue, France. Both offshore and inner surf zone measurements are provided to quantify the incoming wave forcing. Continuous high-frequency swash zone measurements are performed thanks to, (i), a 2-dimensional laser scanner (LiDAR) to follow free surface and sand bed dynamics and, (ii), a cross-shore array of 15 buried pressure sensors to study groundwater properties. By contrast to, for example, (Heiss et al., 2015) the focus is mainly made here on the permanently saturated zone under the swash zone and the presented data are, to the best of the authors knowledge, a first field evidence of groundwater circulation under the swash zone.

Measurements started during a moderate storm (in the Mediterranean context) associated to a significant rise of the mean water level, which provides a complete inundation of the measurement area. The storm decay induces a MWL lowering and a decrease of wave activity, allowing to monitor the swash zone/watertable retreat and its impact on groundwater dynamics. Three phases are selected to highlight the evolution of the groundwater pressure field and Darcy-related flow into the soil. A time-averaged analysis demonstrates the presence of a rather consistent groundwater circulation pattern under the swash zone, shifting offshore with the swash zone. The overall trend, which is in good agreement with the laboratory observations of Turner et al. (2016), is a seaward groundwater flow, with a maximal intensity about 0.1 mm/s, modulated by infiltration/exfiltration in the upper/lower swash zones.

The statistical analysis of groundwater flow shows some interesting features: vertical flows are greater than horizontal ones, mainly negative (infiltration) and greater close to the sand surface while horizontal components are nearly systematically seaward and greater in the lower swash zone. Two time-resolved swash events measured during Phase 1 (high swash zone) and 3 (low swash zone) are thus compared to draw the main features of the instantaneous groundwater response to a typical uprush/backwash cycle. The general scheme is, (i), a nearly hydrostatic groundwater pressure under the dry area of the beach, (ii), an overall infiltration flow during the bed inundation by the swash tongue, (iii), a seaward groundwater flow during the swash retreat and, (iv), a localized exfiltration flow under the next incoming uprush, strictly observed during long backwash events on a saturated bed.

Although the measurements have been carried out during the peak and decay of a moderate storm and in a microtidal context, the present observations may remain valid in a much wider range of conditions. Further field campaigns should be planned in particular when considering meso and macro-tidal conditions for which beach saturation fluctuations (Heiss et al., 2015) and subsurface circulation must combine to control the groundwater fluxes. Our observations should also be of great importance when analysing less resolved field data (e.g. piezometres are not able to reveal any vertical motion) and/or when studying fluxes of dissolved materials or contaminants or bio-geochemical processes in coastal aquifers.

Acknowledgements

This study was sponsored by the Direction Departementale Territoriale et Maritime 13 and the ANR Grant No. ANR-13-ASTR-0007. We thank the Parc Naturel Rgional de Camargue, Reserve

Naturelle de Camargue and the municipality of Saintes-Maries-de-la-Mer for technical assistance and autorization to access the beach. The GLADYS group (www.gladys-littoral.org) supported the experimentation. We are grateful to all the contributors involved in this experiment. The authors are particularly indebted to Sébastien Marguerite whose efforts were essential to the deployment.

References

Almeida, L., Masselink, G., Russell, P., Davidson, M., 2015. Observations of gravel beach dynamics during high energy wave conditions using a laser scanner. Geomorphology 228, 15–27.

Anschutz, P., Smith, T., Mouret, A., Deborde, J., Bujan, S., Poirier, D., Lecroart, P., 2009. Tidal sands as biogeochemical reactors. Estuarine Coast. Shelf Sci. 84 (1), 84–90.

Austin, M.J., Masselink, G., 2006. Swash–groundwater interaction on a steep gravel beach. Continent. Shelf Res. 26 (20), 2503–2519.

Blenkinsopp, C., Mole, M., Turner, I., Peirson, W., 2010. Measurements of the time–varying free-surface profile across the swash zone obtained using an industrial LIDAR. Coast. Eng. 57 (11), 1059–1065.

Burnett, W., Aggarwal, P., Aureli, A., Bokuniewicz, H., Cable, J., Charette, M., Kontar, E., Krupa, S., Kulkarni, K., Loveless, A., et al., 2006. Quantifying submarine groundwater discharge in the coastal zone via multiple methods. Sci. Total Env. 367 (2), 498–543.

Butt, T., Russell, P., Turner, I., 2001. The influence of swash infiltration–exfiltration on beach face sediment transport: Onshore or offshore? Coast. Eng. 42 (1), 35–52.

Cartwright, N., Nielsen, P., Li, L., 2004. Experimental observations of watertable waves in an unconfined aquifer with a sloping boundary. Adv. Water Resour. 27 (10), 991–1004.

Charbonnier, C., Anschutz, P., Poirier, D., Bujan, S., Lecroart, P., 2013. Aerobic respiration in a high-energy sandy beach. Mar. Chem. 155, 10–21.

Chardón-Maldonado, P., Pintado-Patiño, J.C., Puleo, J.A., 2015. Advances in swash-zone research: Small-scale hydrodynamic and sediment transport processes. Coast. Eng.. http://dx.doi.org/10.1016/j.coastaleng.2015.10.008.

Conley, D.C., Inman, D.L., 1994. Ventilated oscillatory boundary layers. J. Fluid Mech. 273, 261–284.

Corvaro, S., Miozzi, M., Postacchini, M., Mancinelli, A., Brocchini, M., 2014a. Fluid—particle interaction and generation of coherent structures over permeable beds: An experimental analysis. Adv. Water Resour. 72, 97–109.

Corvaro, S., Seta, E., Mancinelli, A., Brocchini, M., 2014b. Flow dynamics on a porous medium. Coast. Eng. 91, 280–298.

De Montety, V., 2008. Salinisation d'un aquifère captif côtier en contexte deltaïque–Cas de la Camargue (delta du Rhône, France)-. Université d'Avignon Ph.D. thesis.

Geng, X., Boufadel, M.C., 2015. Numerical study of solute transport in shallow beach aquifers subjected to waves and tides. J. Geophys. Res. 120 (2), 1409–1428.

Hegge, B.J., Masselink, G., 1991. Groundwater-table responses to wave run-up: An experimental study from western australia. J. Coast. Res. 623–634.

Heiss, J.W., Puleo, J.A., Ullman, W.J., Michael, H.A., 2015. Coupled surface-subsurface hydrologic measurements reveal infiltration, recharge, and discharge dynamics across the swash zone of a sandy beach. Water Resour. Res.. http://dx.doi.org/10.1002/2015WR017395.

Heiss, J.W., Ullman, W.J., Michael, H.A., 2014. Swash zone moisture dynamics and unsaturated infiltration in two sandy beach aquifers. Estuarine Coast. Shelf Sci. 143, 20–31.

Horn, D.P., 2006. Measurements and modelling of beach groundwater flow in the swash-zone: A review. Continent. Shelf Res. 26 (5), 622–652.

Kang, H.-Y., Nielsen, P., Hanslow, D.J., 1994. Watertable overheight due to wave runup on a sandy beach. Coast. Eng. Proc. 1 (24).

Karambas, T.V., 2003. Modelling of infiltration-exfiltration effects of cross-shore sediment transport in the swash zone. Coast. Eng. J. 45 (01), 63–82.

Klute, A., Dirksen, C., 1986. Hydraulic conductivity and diffusivity: laboratory methods. Methods Soil Anal. 687–734.

Li, L., Barry, D., 2000. Wave-induced beach groundwater flow. Adv. Water Resour. 23 (4), 325–337.

Lofi, J., Pezard, P., Bouchette, F., Raynal, O., Sabatier, P., Denchik, N., Levannier, A., Dezileau, L., Certain, R., 2013. Integrated onshore-offshore investigation of a mediterranean layered coastal aquifer. Groundwater 51 (4), 550–561.

Longuet-Higgins, M.S., 1983. Wave set-up, percolation and undertow in the surf zone. In: Proceedings of the Royal Society of London A: Mathematical, Physical and Engineering Sciences, vol. 390. The Royal Society, pp. 283–291.

Martins, K., Blenkinsopp, C., Zang, J., 2015. Monitoring individual wave characteristics in the inner surf with a 2-dimensional laser scanner (liDAR). J. Sensors ID 461379 (2016).

McAllister, S.M., Barnett, J.M., Heiss, J.W., Findlay, A.J., MacDonald, D.J., Dow, C.L., Luther, G.W., Michael, H.A., Chan, C.S., 2015. Dynamic hydrologic and biogeochemical processes drive microbially enhanced iron and sulfur cycling within the intertidal mixing zone of a beach aquifer. Limnol. Oceanography 60 (1), 329–345.

Nielsen, P., 1990. Tidal dynamics of the water table in beaches. Water Resour. Res. 26 (9), 2127–2134.

Ouahsine, A., Smaoui, H., Meftah, K., Sergent, P., Sabatier, F., 2013. Numerical study of coastal sandbar migration, by hydro-morphodynamical coupling. Env. Fluid. Mech. 13, 169–187.

Robinson, C., Gibbes, B., Li, L., 2006. Driving mechanisms for groundwater flow and salt transport in a subterranean estuary. Geophys. Res. Lett. 33 (3).

Sabatier, F., 2001. Fonctionnement et dynamiques morpho-sédimentaires du littoral du delta du Rhône. Université d'Aix-Marseille III Ph.D. thesis.

Sabatier, F., 2008. Modélisation de l'impact du changement climatique sur l'érosion des dunes. application à la camargue. La Houille Blanche (1) 40–49.

Sabatier, F., Anthony, E.J., Héquette, A., Suanez, S., Musereau, J., Ruz, M.-H., Régnauld, H., 2009a. Morphodynamics of beach/dune systems: Examples from the coast of france. Géomorphologie: relief, processus, environnement (1/2009) 3–22.

Sabatier, F., Samat, O., Ullmann, A., Suanez, S., 2009b. Connecting large-scale coastal behaviour with coastal management of the rhône delta. Geomorphology 107 (1), 79–89.

Sawyer, A.H., Lazareva, O., Kroeger, K.D., Crespo, K., Chan, C.S., Stieglitz, T., Michael, H.A., 2014. Stratigraphic controls on fluid and solute fluxes across the sediment-water interface of an estuary. Limnol. Oceanogr. 59 (3), 997–1010.

Shoushtari, S.M.H.J., Cartwright, N., Nielsen, P., Perrochet, P., 2015. The effects of oscillation period on groundwater wave dispersion in a sandy unconfined aquifer: Sand flume experiments and modelling. J. Hydrol.. http://dx.doi.org/10.1016/j.jhydrol.2015.12.032.

Sibson, R., 1981. A brief description of natural neighbour interpolation. Interpreting Multivariate Data.

Sous, D., Lambert, A., Rey, V., Michallet, H., 2013. Swash–groundwater dynamics in a sandy beach laboratory experiment. Coast. Eng. 80, 122–136.

Steenhauer, K., Pokrajac, D., O'Donoghue, T., Kikkert, G., 2011. Subsurface processes generated by bore-driven swash on coarse-grained beaches. J. Geophys. Res. 116 (C4).

Turner, I., 1993. Water table outcropping on macro-tidal beaches: a simulation model. Mar. Geol. 115 (3), 227–238.

Turner, I.L., 1998. Monitoring groundwater dynamics in the littoral zone at seasonal, storm, tide and swash frequencies. Coast. Eng. 35 (1), 1–16.

Turner, I.L., Coates, B.P., Acworth, R.I., 1997. Tides, waves and the super-elevation of groundwater at the coast. J. Coast. Res. 46–60.

Turner, I.L., GC, R., MJ, A., MS, A., 2016. Groundwater fluxes and flow paths within coastal barriers: Observations from a large-scale laboratory experiment (BARDEX II). Coast. Eng.. http://dx.doi.org/10.1016/j.coastaleng.2015.08.004.

Turner, I.L., Masselink, G., 1998. Swash infiltration-exfiltration and sediment transport. J. Geophys. Res. 103 (C13), 30813–30824.

Turner, I.L., Masselink, G., 2012. Coastal gravel barrier hydrology-observations from a prototype-scale laboratory experiment (BARDEX). Coast. Eng. 63, 13–22.

Turner, I.L., Nielsen, P., 1997. Rapid water table fluctuations within the beach face: implications for swash zone sediment mobility? Coast. Eng. 32 (1), 45–59.

Waddell, E., 1973. Dynamics of Swash and Implication to Beach Response.. DTIC Document Tech. rep.

Waddell, E., 1980. Wave forcing of beach groundwater. Coast. Eng. Proc. (17).

Wilson, B., 1972. Seiches. Adv. Hydrosci. 8, 1–94.